Design Proposal: Mach-Zehnder Interferometer

William Boucher
edX: UBCX PHOT1X, Silicon Photonics Design

***Abstract*—This report presents five unbalanced Mach-Zehnder interferometer (MZI) designs for the SiEPIC EBeam 220 nm silicon-on-insulator platform. The designs cover path length differences from 10.2 to $161.1\,\mu\mathrm{m}$, giving free spectral ranges (FSR) from roughly 4 to $56\,\mathrm{nm}$ across the C-band. Two topologies are explored: a Y-branch with a broadband directional coupler (BDC), and a symmetric dual Y-branch (Y-Y) configuration. Circuit-level simulations with FDTD-derived compact models confirm the expected inverse relationship between path difference and FSR. The extracted group index values are consistent with the PDK reference of $n_g = 4.19$.**

I. Introduction

Silicon photonics takes advantage of well-established CMOS fabrication to bring optical functions onto a single chip, opening the door to high-bandwidth interconnects, integrated sensors, and compact signal processors [1], [2]. One of the most common building blocks in this space is the Mach-Zehnder interferometer (MZI). It works by splitting an input optical field into two waveguide arms, letting each arm pick up a different phase, and then recombining them so the output depends on wavelength [3].

When the two arms have different physical lengths, the transmission spectrum shows periodic fringes. The spacing between those fringes, called the free spectral range (FSR), is inversely proportional to the path length difference ΔL and scales with the group index n_g of the waveguide. This means that by measuring the FSR of an unbalanced MZI, one can extract n_g directly from the spectrum, which is useful for characterising waveguides and calibrating designs.

In this work, five MZI variants were designed on the SiEPIC EBeam PDK targeting a 220 nm SOI platform [4]. The set includes one design that pairs a Y-branch splitter with a broadband directional coupler (BDC-MZI), giving two complementary output channels, and four designs that use a symmetric dual Y-branch (Y-Y) topology with a single through port. All simulations rely on FDTD-derived compact models from the PDK rather than idealised analytical formulas, which turned out to make a significant difference in accuracy.

II. Theory

A. MZI Transfer Function

For an MZI with ideal 50:50 splitting, the input field E_i is divided equally at the input coupler:

$$E_{a,1} = \frac{E_i}{\sqrt{2}}, \qquad E_{a,2} = \frac{E_i}{\sqrt{2}}. \tag{1}$$

Each field then propagates through a waveguide of length L_j with propagation constant $\beta = 2\pi\, n_{\text{eff}}(\lambda)/\lambda$, picking up phase βL_j along the way. After recombination at the output coupler, the total field is

$$E_o = \frac{E_i}{2}\left(e^{-i\beta L_1} + e^{-i\beta L_2}\right), \tag{2}$$

and the normalised output intensity becomes

$$T = \frac{I_o}{I_i} = \frac{1}{2}\left[1 + \cos(\beta\,\Delta L)\right], \tag{3}$$

where $\Delta L = L_1 - L_2$. The output hits a maximum whenever $\beta\,\Delta L = 2m\pi$ (constructive interference) and drops to zero when $\beta\,\Delta L = (2m+1)\pi$ (destructive interference).

B. Free Spectral Range

The FSR is the wavelength gap between consecutive transmission peaks. Starting from the accumulated phase $\delta = 2\pi\, n_{\text{eff}}\,\Delta L/\lambda$ and requiring that two neighbouring maxima satisfy $\delta_m - \delta_{m+1} = 2\pi$, a first-order Taylor expansion of $\beta(\lambda)$ gives

$$\frac{d\beta}{d\lambda} = -\frac{2\pi n_g}{\lambda^2}, \tag{4}$$

with the group index defined as

$$n_g = n_{\text{eff}} - \lambda\,\frac{dn_{\text{eff}}}{d\lambda}. \tag{5}$$

Plugging this back in leads to the well-known FSR formula:

$$\text{FSR} = \frac{\lambda^2}{n_g \cdot \Delta L}. \tag{6}$$

If the group index is not known ahead of time, (6) can be flipped around to extract it from a measured spectrum:

$$n_g = \frac{\lambda^2}{\text{FSR} \cdot \Delta L}. \tag{7}$$

C. Effect of Coupler Dispersion

Equation (6) assumes that the couplers themselves do not add any wavelength-dependent phase. This is a reasonable assumption for the Y-Y topology, where both couplers are broadband Y-branches with nearly flat splitting. However, in the BDC-MZI topology, the directional coupler introduces its own wavelength-dependent phase between the bar and cross paths. This extra dispersive phase shifts the effective optical path difference seen by the interferometer, so the simple formula becomes only an approximation. To get accurate results in this case, the full S-parameter matrix of the BDC needs to be included [5], which is one of the main reasons FDTD-based models were used here.

TABLE I
STRIP WAVEGUIDE PARAMETERS AT $\lambda = 1550\,\mathrm{nm}$.

Parameter	Symbol	Value
Effective index (TE)	n_{eff}	2.44553
Group index (TE)	n_g	4.19088
Propagation loss	α	$3\,\mathrm{dB/cm}$
Core dimensions	$w \times h$	$500\,\mathrm{nm} \times 220\,\mathrm{nm}$
Core / cladding		Si / SiO_2

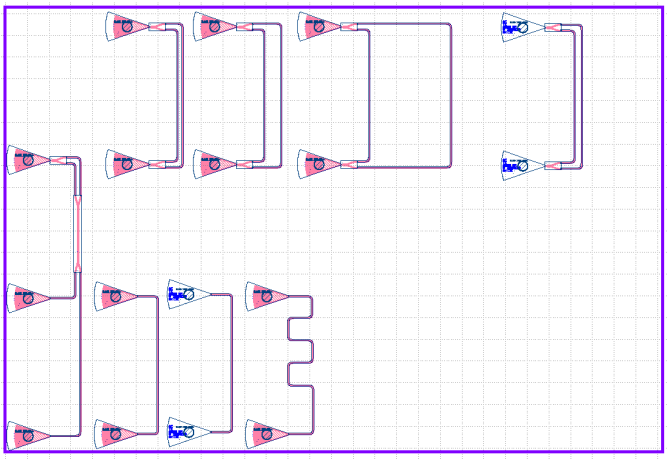

Fig. 1. Full chip layout of `EBeam_w-boucher_v2.gds`, rendered in KLayout. The five MZI designs are arranged with grating coupler I/O along the chip edges.

III. DESIGN

A. Platform and Components

All five designs were built on the SiEPIC EBeam PDK (v0.5.31), which targets a 220 nm SOI platform [4]. The waveguides are fully etched silicon strips with a $500\,\mathrm{nm} \times 220\,\mathrm{nm}$ cross-section, supporting a single TE mode at $1550\,\mathrm{nm}$. Table I lists the key waveguide parameters taken from the FDTD simulation data bundled with the PDK.

Three PDK components appear across the designs. The grating coupler (`ebeam_gc_te1550`) provides fibre-to-chip coupling with roughly $2.3\,\mathrm{dB}$ insertion loss at $1550\,\mathrm{nm}$. The Y-branch (`ebeam_y_1550`) is a 3-port splitter with $|S_{21}| = |S_{31}| \approx 0.694$, giving near-ideal 50:50 splitting and about $0.3\,\mathrm{dB}$ excess loss. The broadband directional coupler (`ebeam_bdc_te1550`) is a 4-port device that also splits close to 50:50 but has a noticeably wavelength-dependent coupling phase.

B. MZI Configurations

The five MZI designs are laid out on a single chip, shown in Fig. 1. Design 1 uses a Y-branch at the input and a BDC at the output, which gives two complementary output channels (bar and cross). Designs 2 through 5 all use the simpler Y-Y topology with one through-port output. Design 5 swaps in oxide-cladded grating couplers (`GC_TE_1550_8degOxide_BB`) for the fibre interface.

TABLE II
MZI DESIGN PARAMETERS AND THEORETICAL FSR.

#	Topology	L_{short} (µm)	ΔL (µm)	$\mathrm{FSR_{th}}$ (nm)
1	BDC-MZI	36.46	10.20	56.2
2	Y-Y MZI	140.70	20.24	28.3
3	Y-Y MZI	140.70	42.10	13.6
4	Y-Y MZI	140.70	161.10	3.6
5	Y-Y (oxide GC)	143.62	24.32	23.6

Table II summarises the arm lengths, path differences, and theoretical FSR for each design, computed from (6).

In Design 1, the input goes through a Y-branch and splits into arms of 46.66 and $36.46\,\mu\mathrm{m}$, which then feed into opposite sides of the BDC. The bar and cross ports of the BDC are routed through waveguides of 45.56 and $177.26\,\mu\mathrm{m}$ to their respective output grating couplers. Designs 2 through 5 are all wired the same way: a Y-branch splits the input into a short arm and a long arm, and a second Y-branch recombines them into a single output.

IV. SIMULATION METHODOLOGY

A. Circuit Simulator

The simulations were run using SAX [6], an open-source photonic circuit simulator that builds up the full circuit S-matrix by composing the individual component matrices. It takes a netlist of instances, connections, and external ports, and evaluates the response at each wavelength. A sweep of 2000 points from 1500 to $1600\,\mathrm{nm}$ was used for all designs.

B. Compact Models

Instead of using hand-written analytical models, the simulations here use FDTD-derived S-parameter data from the SiEPIC PDK [4]. These compact models capture the full complex transmission and reflection as a function of frequency, including wavelength-dependent coupling ratios and phase shifts that simple formulas would miss. The waveguide is modelled with a first-order dispersion relation using the n_{eff} and n_g values from the PDK, along with $3\,\mathrm{dB/cm}$ propagation loss. The grating coupler, Y-branch, and BDC models are loaded from tabulated files (51 to 101 frequency points each) and interpolated with cubic splines onto the simulation wavelength grid.

C. Netlist Extraction

One practical challenge was that the GDS layout from SiEPIC-Tools does not expose a netlist that can be read programmatically. The circuit connectivity had to be reconstructed by hand: inspecting the cell hierarchy to find component instances, reading waveguide lengths from SPICE parameter labels on GDS layer 68/0, pulling optical pin positions from layer 1/10, and then matching up the global coordinates to figure out which ports connect to which. This was done separately for each of the five designs.

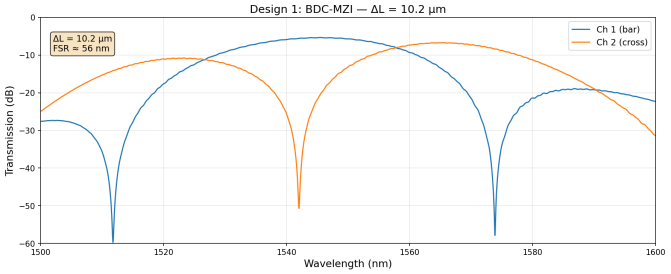

Fig. 2. Transmission of Design 1 (BDC-MZI, $\Delta L = 10.2\,\mu\text{m}$). The bar channel (blue) and cross channel (orange) show complementary interference patterns.

TABLE III
THEORETICAL VS. SIMULATED FSR AND EXTRACTED GROUP INDEX.

#	ΔL (µm)	FSR_{th} (nm)	FSR_{sim} (nm)	$n_{g,\text{ext}}$
1	10.20	56.2	∼56	∼4.20
2	20.24	28.3	∼29	∼4.09
3	42.10	13.6	∼14	∼4.08
4	161.10	3.6	∼4	∼3.72
5	24.32	23.6	∼24	∼4.12

V. Simulation Results

A. BDC-MZI (Design 1)

Fig. 2 shows the simulated spectrum of Design 1. The bar and cross outputs are clearly complementary: when one channel peaks, the other dips, which is what you would expect from power conservation in a 4-port coupler. The measured FSR comes out to about $56\,\text{nm}$, matching the theoretical value of $56.2\,\text{nm}$ very well. Peak transmission sits around $-6\,\text{dB}$, which makes sense given the $\sim 2.3\,\text{dB}$ loss from each of the two grating couplers plus a small amount of component excess loss. The extinction ratio at the deepest nulls exceeds $40\,\text{dB}$.

B. Y-Y MZI Designs (2 to 5)

Fig. 3 shows the through-port spectra for all four Y-Y designs. The trend is exactly what (6) predicts: as ΔL gets larger, the fringes become more closely spaced. Design 2 ($\Delta L = 20.24\,\mu\text{m}$) has about 3 full periods across the 100 nm window, while Design 4 ($\Delta L = 161.1\,\mu\text{m}$) packs in dense fringes with an FSR of roughly $4\,\text{nm}$. All four designs show extinction ratios above $40\,\text{dB}$, and the overall spectral shape follows the Gaussian-like envelope of the grating coupler, peaking near $1550\,\text{nm}$ and rolling off toward the band edges.

C. Comparative Overview

Fig. 4 overlays all five designs on a linear power scale. The grating coupler envelope is clearly visible as the common ceiling that bounds the transmission of every device.

Table III puts the theoretical and simulated FSR values side by side and includes the group index back-calculated from the simulation using (7).

The extracted n_g values all fall in the 4.0 to 4.2 range, which lines up well with the PDK reference of 4.19. The small deviations mostly come down to the limited precision

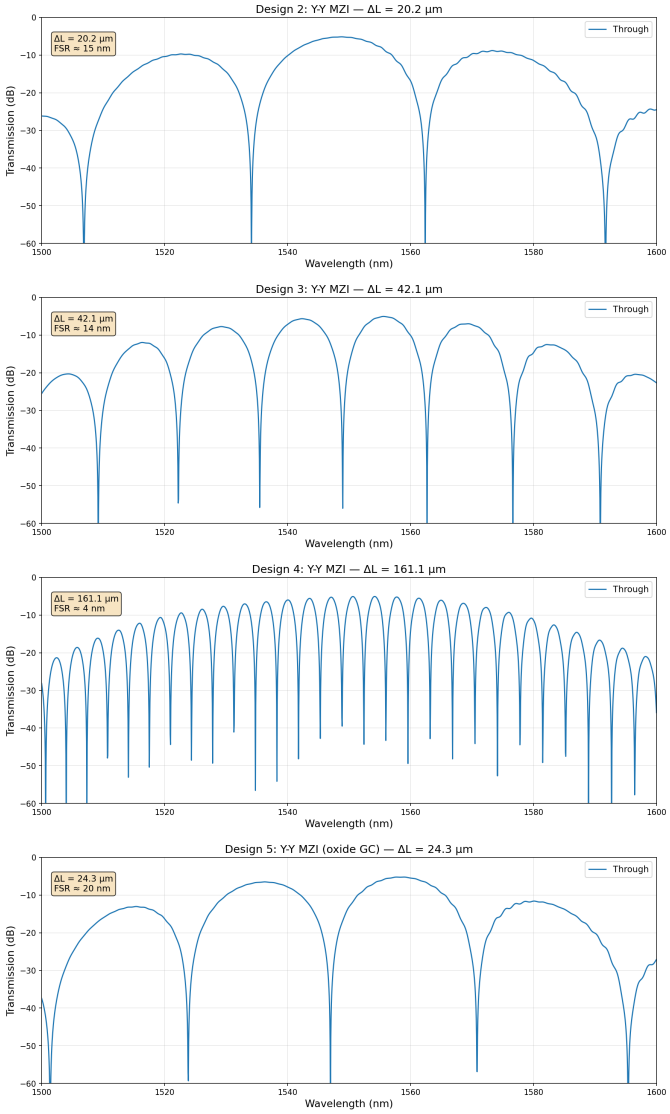

Fig. 3. Transmission spectra of Designs 2 to 5 (Y-Y MZI, top to bottom). ΔL values: 20.24, 42.10, 161.10, and $24.32\,\mu\text{m}$. The fringe density grows with ΔL.

of reading FSR off the simulated spectra and the dispersive phase that the couplers add on top of the pure waveguide contribution.

D. Why FDTD-Based Models Matter

Early on in this project, the simulation used analytical component models with textbook-style parameters ($n_{\text{eff}} = 2.38$, $n_g = 4.30$, flat 50:50 splitting everywhere). The resulting FSR values were noticeably off compared to what Lumerical INTERCONNECT gave for the same circuit. It turned out the problem had two parts: the analytical waveguide model was using effective and group index values that were a few percent away from the calibrated FDTD numbers, and the idealised BDC model completely ignored the wavelength-dependent phase the real coupler picks up. Once the simulation switched to the FDTD compact models from the SiEPIC PDK,

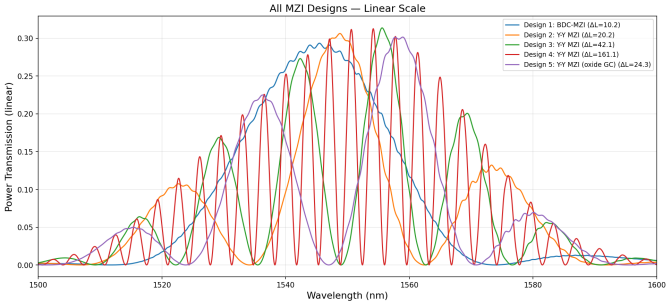

Fig. 4. Linear-scale overlay of all five designs. The shared grating coupler envelope peaks near $1550\,\mathrm{nm}$.

both issues went away. This was a good reminder that in interferometric circuits, where the output is extremely sensitive to phase, even small parameter errors at the component level can cascade into qualitatively wrong results at the circuit level [3].

E. BDC Dispersive Phase

The Y-branch has a fairly flat response across the C-band, so it behaves close to an ideal splitter. The BDC, on the other hand, has both a coupling ratio and a through-path phase that shift with wavelength. This dispersive phase adds an extra wavelength-dependent term to the interferometer's total phase difference, which is why the BDC-MZI does not follow the simple formula of (6) as cleanly as the Y-Y designs do. That said, the BDC topology has the advantage of giving two complementary outputs, which can be useful for balanced detection and noise rejection in sensing setups [5].

F. Design Trade-Offs

The five designs cover a broad range of FSR values, and each end of the spectrum has its own pros and cons. A large FSR like Design 1's ($\sim 56\,\mathrm{nm}$) is good for broadband switching or coarse wavelength filtering, since a single fringe period spans most of the grating coupler bandwidth. A moderate FSR (Designs 2, 3, 5) works well for group index extraction, where having several fringes in the measurement window lets you average out noise. A very fine FSR like Design 4's ($\sim 4\,\mathrm{nm}$) gives high spectral resolution, but you need a correspondingly sharp measurement setup to resolve the fringes. It is also worth noting that designs with longer ΔL are more sensitive to fabrication variations, because phase errors accumulate over longer path lengths.

VI. Fabrication

to fill in later

VII. Experimental Data

to fill in later

VIII. Analysis

to fill in later

A. Limitations

A few caveats should be kept in mind. The oxide-cladded grating coupler used in Design 5 was approximated with the standard air-cladded GC S-parameter data, since the oxide GC model was not available. The actual coupling envelope and insertion loss may differ. There is also no fabrication or measurement data yet to validate these simulations against real devices. Finally, the waveguide loss model is a simple constant of $3\,\mathrm{dB/cm}$ and does not capture effects like bend loss or local sidewall roughness variations.

IX. Conclusion

to fill in later

References

[1] D. Thomson *et al.*, "Roadmap on silicon photonics," *J. Opt.*, vol. 18, no. 7, p. 073003, 2016.
[2] R. Soref, "The past, present, and future of silicon photonics," *IEEE J. Sel. Top. Quantum Electron.*, vol. 12, no. 6, pp. 1678–1687, 2006.
[3] L. Chrostowski and M. Hochberg, *Silicon Photonics Design: From Devices to Systems*. Cambridge, UK: Cambridge Univ. Press, 2015.
[4] SiEPIC, "SiEPIC EBeam PDK," GitHub. [Online]. Available: https://github.com/SiEPIC/SiEPIC_EBeam_PDK
[5] Z. Lu *et al.*, "Broadband silicon photonic directional coupler using asymmetric-waveguide based phase control," *Opt. Express*, vol. 23, no. 3, pp. 3795–3808, 2015.
[6] F. Laporte, "SAX: S-parameter Analyzer in jaX," GitHub. [Online]. Available: https://github.com/flaport/sax
[7] W. Bogaerts *et al.*, "Silicon microring resonators," *Laser Photonics Rev.*, vol. 6, no. 1, pp. 47–73, 2012.